(Received 8 April 2026, Accepted 13 May 2026, Scheduled 1 June 2026)

Accurate Calculation of Mutual Inductance for Rounded Rectangular Coils in Arbitrary Orientations in Wireless Power Transfer Systems

Zhongjiu Zheng, Minghao Zhao*, Zhuang Li, Xingfeng Cao, and Anran Liu

College of Marine Electrical Engineering, Dalian Maritime University, Dalian 116026, China

ABSTRACT: This paper proposes a semi-analytical method for arbitrary spatial orientations that eliminates systematic errors arising from neglecting rounded corners in planar rectangular coils in wireless power transfer systems. The rounded rectangular coil is decomposed into straight and quarter-arc segments. Using Neumann's formula, mutual inductance expressions for straight-straight, straight-arc, and arc-arc interactions are derived. We establish a unified spatial model using Z-Y-X Euler angle transformations to describe arbitrary translations and rotations in 3D space. We obtain the total mutual inductance by superposition. Results show that neglecting rounded corners increases error as the corner radius grows. Under various conditions, including lateral and axial displacements and composite rotations, the method achieves average relative errors below 1.5% compared with finite element simulations (validated for corner radii up to 12 mm) and below 2.5% compared with experiments (validated for a corner radius of 5 mm), demonstrating high accuracy and robustness. A single configuration takes about 2 seconds in MATLAB, compared to 20–30 minutes in FEM.

1. INTRODUCTION

Wireless power transfer (WPT) is an emerging power transmission technology that has been widely applied in various fields [1], such as communication applications [2], biomedical sensing [3], and micro-robot propulsion [4]. WPT systems primarily rely on magnetic field coupling, whereby power is transmitted wirelessly from the transmitter to the receiver. This method enables contactless power transfer through interacting electromagnetic fields; therefore, mutual inductance plays a crucial role in the design and performance evaluation of WPT systems.

Figure 1 shows the basic framework of a typical inductively coupled wireless power transfer system. The system includes a power source, a high-frequency H-bridge inverter, a compensation network, primary and secondary coils, a rectifier, and a load [5]. The primary and secondary coils interact via magnetic fields, transferring power from the primary to the secondary, and the rectifier circuit then converts this power into DC.

Among WPT system components, planar coils, as the core components of WPT systems, have become the most commonly used coupling elements due to their compact structure and high adaptability [6–8]. However, in practice, wire flexibility and manufacturing limitations inevitably result in rounded corners when rectangular coils are wound [9]. Simply approximating these coils as ideal rectangles introduces systematic errors that affect transmission efficiency and the accuracy of design optimization in WPT systems [10, 11]. Therefore, accurately calculating the mutual inductance of rounded rectangular coils in arbitrary orientation is a key to improving the design precision of WPT systems.

To date, extensive research has been conducted on the calculation of mutual inductance for planar coils. Liu et al. derived an exact expression for mutual inductance applicable to any relative orientation by introducing Euler angles to describe all six degrees of freedom in three-dimensional space. Experiments verified its high accuracy under misalignment [12]. Altun and Pirinççi extended their research to planar coils with arbitrary regular polygonal shapes, proposing a general analytical model based on magnetic vector potential and coordinate transformations [13]. Li et al. proposed a mutual inductance calculation method applicable to rectangular coils positioned at arbitrary locations within a magnetic medium [14]. They derived the mutual inductance expressions using the spatial cross-section analysis method and the mirror constraint method, verified their validity through experiments, and demonstrated material savings compared to traditional rectangular magnetic medium structures [15]. Recently, Wu and Feng proposed a second-order vector potential method for perpendicular rounded rectangular coils, but their approach does not extend to arbitrary 3D orientations [16].

Most studies have focused on coils with regular shapes or have limited their simulation analyses to treating rounded corners as optimization variables [17–19]. There remains a lack of a general analytical mutual inductance model specifically tailored to the irregular geometry of rounded rectangular coils [20].

To establish a fundamental analytical framework and validate its core geometric decomposition approach, we focus on

* Corresponding author: Minghao Zhao (952049449@qq.com).

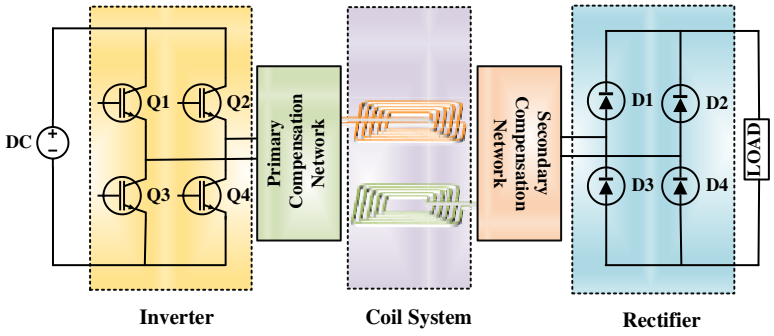

FIGURE 1. Wireless power transmission system.

air-core coils, which serve as the building blocks for more complex systems. The remainder of this paper is organized as follows. First, we model the multi-turn, rounded rectangular coil as a set of concentric single-turn thin-wire loops, define its geometric parameters, and introduce a Z-Y-X Euler angle coordinate transformation framework. This framework uniformly describes the arbitrary translation and rotation of the primary and secondary coils in three-dimensional space. Based on this framework, we compare our analytical results with finite element simulations and experimental measurements to verify the accuracy and validity of the proposed model under various displacements and composite rotations. Finally, we summarize the paper.

2. ANALYTICAL CALCULATION OF PLANAR ROUNDED RECTANGULAR COILS

2.1. Coil Model and Parameter Definition

To build a model for calculating mutual inductance under arbitrary spatial positions and orientations, we approximate the spiral coil as a set of concentric single-turn coils. A single-turn, rounded rectangular coil is equivalent to a closed loop of four straight segments and four quarter-arc segments connected end to end. Fig. 2 shows the equivalent model.

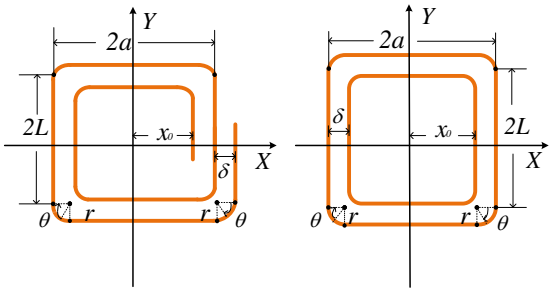

FIGURE 2. Rounded rectangular coil equivalent model.

Because the coil has a finite cross-sectional area, and the wire cross-section is much smaller than both the coil dimensions and inter-coil distance, we assume that the current flows along the geometric centerline of the wire. Using the thin-wire approximation, the parameters of the equivalent coil are defined as follows:

Half-side length of the rounded rectangle: a,

Starting position of the coil: x,

Rounded corner radius: r,

Straight segment length: $L = 2(a - r)$,

Pitch: δ (center-to-center distance between adjacent turns in the radial direction),

Number of turns: N.

For a coil consisting of N turns, we treat each turn as an independent closed, rounded rectangular loop. During the spiral winding process, the size gradually increases with each outward turn, as shown in Fig. 3. We assume that the geometric shape remains similar for all turns. Specifically, for the i-th turn, the half-side length $a_{(i)}$ and rounded corner radius $r_{(i)}$ are given by:

$$\begin{aligned} a_{(i)} &= a + (i-1)\delta \\ r_{(i)} &= r + (i-1)\delta \end{aligned} \tag{1}$$

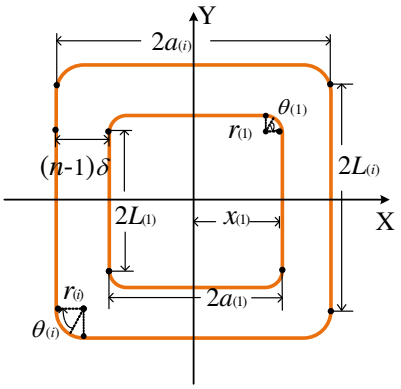

FIGURE 3. Schematic diagram of N-turn rounded rectangular coil structure.

The thin-wire approximation holds when the distance between any two filament segments is much larger than the wire radius [21]. In all our experimental and simulated cases, the minimum center-to-center distance between wires is at least 10 times the wire diameter, making the thin-wire error negligible. Based on the test cases in Table 2 and Table 3, we empirically establish the following quantitative criterion: for $d/w > 10$ the thin-wire error is negligible. Based on the test cases in Table 4 for $d/w < 5$, a geometric mean distance (GMD) correction is recommended.

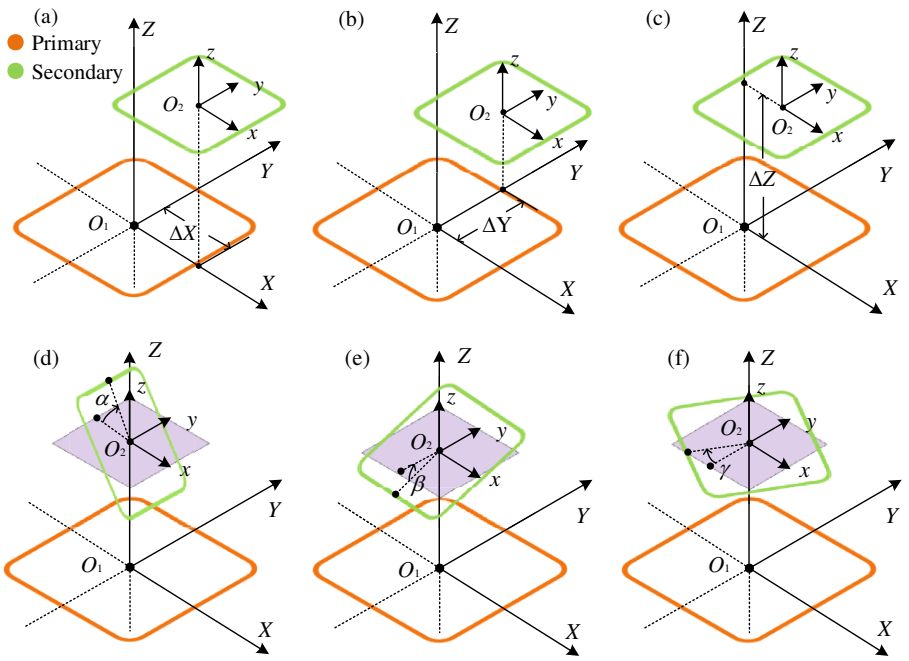

FIGURE 4. Six cases of coil misalignment: (a) displacement along the X-axis, (b) displacement along the Y-axis, (c) displacement along the Z-axis, (d) rotation about the X-axis, (e) rotation about the Y-axis, (f) rotation about the Z-axis.

To describe arbitrary relative positions and orientations between two coils in 3D space, we fix one coil at the origin and call it the primary coil with its reference coordinate system $\{O_1, X, Y, Z\}$. We call the other coil (positioned above) the secondary coil with its local coordinate system $\{O_2, \zeta, \xi, \eta\}$. Both coils have clockwise current directions.

As shown in Fig. 4, we decompose these six parameters into translation and rotation components, which together define the coil's position and orientation. From top to bottom and left to right, the parameters represent the displacements of the secondary coil along the X-axis, Y-axis, and Z-axis of the reference coordinate system, denoted as $\Delta X, \Delta Y, \Delta Z$, respectively. The translation vector $\mathbf{T}$ is defined accordingly. The rotation angles about the reference X-axis, Y-axis, and Z-axis are denoted as α, β, γ.

We use the Z-Y-X Euler angle order for the rotation matrix $\mathbf{R}$. The rotation matrix $\mathbf{R}$ and translation vector $\mathbf{T}$ are expressed as:

$$\mathbf{R} = \begin{bmatrix} R_{11} & R_{12} & R_{13} \\ R_{21} & R_{22} & R_{23} \\ R_{31} & R_{32} & R_{33} \end{bmatrix}, \quad \mathbf{T} = \begin{bmatrix} \Delta X \\ \Delta Y \\ \Delta Z \end{bmatrix} \tag{2}$$

The rotation matrix is given by:

$$\mathbf{R} = \mathbf{R}_z(\gamma)\mathbf{R}_y(\beta)\mathbf{R}_x(\alpha) \tag{3}$$

The basic rotation matrices $\mathbf{R}_x(\alpha), \mathbf{R}_y(\beta), \mathbf{R}_z(\gamma)$ are respectively:

$$\mathbf{R}_x(\alpha) = \begin{pmatrix} 1 & 0 & 0 \\ 0 & \cos\alpha & -\sin\alpha \\ 0 & \sin\alpha & \cos\alpha \end{pmatrix},$$

$$\mathbf{R}_y(\beta) = \begin{pmatrix} \cos\beta & 0 & \sin\beta \\ 0 & 1 & 0 \\ -\sin\beta & 0 & \cos\beta \end{pmatrix}, \tag{4}$$

$$\mathbf{R}_z(\gamma) = \begin{pmatrix} \cos\gamma & -\sin\gamma & 0 \\ \sin\gamma & \cos\gamma & 0 \\ 0 & 0 & 1 \end{pmatrix}$$

The transformation formula from a point $\mathbf{r}_2(x, y, z)$ in the local coordinate system of the secondary coil to the primary coil coordinate system $\mathbf{r}_2'(x', y', z')$ is:

$$\mathbf{r}_2'(x', y', z') = \mathbf{R}\mathbf{r}_2(x, y, z) + \mathbf{T} \tag{5}$$

2.2. Semi-Analytical Calculation of Mutual Inductance of Coils

For the straight segments, we express the vector of the i-th straight segment of the primary coil using Eq. (6). Eq. (7) gives the starting point $\mathbf{p}_1^{(i)}$ of this segment in the primary coil coordinate system, with the right side straight segment taken as the starting point and counting clockwise. The direction vector $\mathbf{v}_1^{(i)}$ can be expressed as shown in Eq. (8).

$$\mathbf{r}_1^{(i)}(t) = \mathbf{p}_1(i) + t\mathbf{v}_1^{(i)}, \; t \in [0, 1] \tag{6}$$

$$\mathbf{p}_1^{(i)} = \begin{cases} [a_1, \, a_1 - r_1, \, 0]^T, & k = 1 \\ [a_1 - r_1, \, -a_1, \, 0]^T, & k = 2 \\ [-a_1, \, -a_1 + r_1, \, 0]^T, & k = 3 \\ [-a_1 + r_1, \, a_1, \, 0]^T, & k = 4 \end{cases} \tag{7}$$

$$\mathbf{v}_1^{(i)} = \begin{cases} [0,\ -L_1,\ 0]^T, & k=1 \\ [-L_1,\ 0,\ 0]^T, & k=2 \\ [0,\ L_1,\ 0]^T, & k=3 \\ [L_1,\ 0,\ 0]^T, & k=4 \end{cases} \tag{8}$$

We parameterize the secondary coil similarly and transform its coordinates into the primary coil coordinate system using Eq. (5):

$$\mathbf{r}_2'^{(j)}(s) = \mathbf{R}\left(\mathbf{p}_2^{(j)} + s\mathbf{R}\mathbf{v}_2^{(j)}\right) + \mathbf{T},\ s \in [0,1] \tag{9}$$

For the arc segments (counting clockwise from the upper-right corner), we write the center coordinates $\mathbf{C}_1^{(k)}$ of the k-th arc segment of the primary coil as:

$$\mathbf{C}_1^{(k)} = \begin{cases} [a_1 - r_1,\ a_1 - r_1,\ 0]^T, & k=1 \\ [a_1 - r_1,\ -a_1 + r_1,\ 0]^T, & k=2 \\ [-a_1 + r_1,\ -a_1 + r_1,\ 0]^T, & k=3 \\ [-a_1 + r_1,\ a_1 - r_1,\ 0]^T, & k=4 \end{cases} \tag{10}$$

The parametric equation $\mathbf{r}_1^{(k)}$ of the k-th arc segment is given by:

$$\mathbf{r}_1^{(k)}(\theta) = \mathbf{C}_1^{(k)} + r_1 \begin{bmatrix} \sin(\theta+\varphi_0) \\ \cos(\theta+\varphi_0) \\ 0 \end{bmatrix} \tag{11}$$

where $\varphi_0 = \frac{\pi}{2}(k-1)$.

For an arbitrary point on an arc segment of the secondary coil, the same approach applies. Combining the transformation formula Eq. (5) with the arc coordinate expression Eq. (11) yields:

$$\mathbf{r}_1'^{(l)}(\phi) = \mathbf{R}\left(\mathbf{C}_2^{(l)} + r_2 \begin{bmatrix} \sin(\phi+\varphi_0) \\ \cos(\phi+\varphi_0) \\ 0 \end{bmatrix}\right) + \mathbf{T} \tag{12}$$

The mutual inductance of rounded rectangular coils is calculated using Neumann's formula:

$$M_{\text{total}} = \sum_{p=1}^{N_1}\sum_{q=1}^{N_2} \frac{\mu_0}{4\pi} \oint_{C_1(p)} \oint_{C_2(q)} \frac{dl_1 \cdot dl_2}{D(r_1, r_2)} \tag{13}$$

where $D(r_1, r_2)$ is the distance function representing the distance between any two points on the segments, and C_1 and C_2 are the closed paths of the p-th and q-th turns, respectively.

We first decompose the single-turn, rounded rectangular coil into four analytically solvable parts: straight-straight mutual inductance M_{LL}, straight-arc mutual inductance M_{LC}, arc-straight mutual inductance M_{CL}, and arc-arc mutual inductance M_{CC}. Then, we sum over all turns to obtain the total mutual inductance between two coils. The summation formula for the mutual inductance M_{ij} of single-turn coils is:

$$M_{ij} = M_{LL} + M_{LC} + M_{CL} + M_{CC} \tag{14}$$

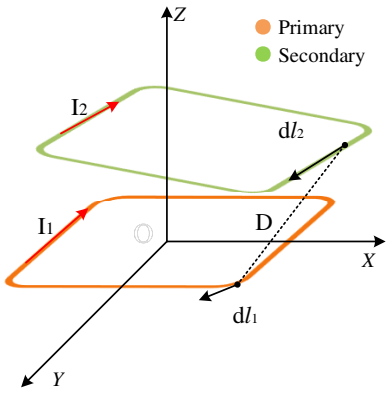

FIGURE 5. Spatial position diagram of a single-turn coil.

For the four cases mentioned above, the tangent direction at any point on each coil is consistent with the current direction, and the distance between two points is denoted by D. The spatial configuration of a single-turn coil is shown in Fig. 5.

For the i-th straight segment of the primary coil and the j-th straight segment of the secondary coil, based on Eqs. (5), (7), and (10), the straight-straight coil mutual inductance is:

$$M_{LL}^{(i,j)} = \frac{\mu_0 \mathbf{v}_1^{(i)} \cdot \left(\mathbf{R}\mathbf{v}_2^{(j)}\right)}{4\pi} \int_0^1 \int_0^1 \frac{dtds}{D_{LL}^{(i,j)}(t,s)} \tag{15}$$

The distance function in Eq. (15) is:

$$\begin{aligned} D_{LL}^{(i,j)}(t,s) &= \left\| \mathbf{r}_1^{(i)}(t) - \mathbf{r}_2'^{(j)}(t) \right\| \\ &= \left\| \left(\mathbf{p}_1^{(i)} + t\mathbf{v}_1^{(i)}\right) - \mathbf{R}\left(\mathbf{p}_2^{(j)} + s\mathbf{R}\mathbf{v}_2^{(j)}\right) - \mathbf{T} \right\| \end{aligned} \tag{16}$$

Because each coil has four straight segments, we sum over all segment combinations to obtain the total straight-straight mutual inductance:

$$M_{LL} = \sum_{i=1}^{4}\sum_{j=1}^{4} M_{LL}^{(i,j)} \tag{17}$$

For the i-th straight segment of the primary coil and the l-th arc segment of the secondary coil, combining Eqs. (7) and (13) yields the straight-arc coil mutual inductance:

$$M_{LC}^{(i,l)} = \frac{\mu_0}{4\pi} \int_0^1 \int_0^{\frac{\pi}{2}} \frac{\mathbf{v}_1^{(i)} \cdot \left(\mathbf{R}\mathbf{t}_2^{(l)}(\phi)\right)\, dtd\phi}{D_{LC}^{(i,l)}(t,\phi)} \tag{18}$$

The tangent vector is expressed as:

$$\mathbf{t}_2^{(l)}(\phi) = \begin{bmatrix} r_2 \cos\left(\phi + \phi_0^{(l)}\right) \\ -r_2 \sin\left(\phi + \phi_0^{(l)}\right) \\ 0 \end{bmatrix} \tag{19}$$

The distance function is:

$$D_{LC}^{(i,l)}(t,\phi) = \left\| \mathbf{r}_1^{(i)}(t) - \mathbf{r}_2'^{(l)}(\phi) \right\| \tag{20}$$

where $\mathbf{r}_2'^{(l)}(\phi)$ is the result from Eq. (12). The total straight-arc mutual inductance is:

$$M_{LC} = \sum_{i=1}^{4}\sum_{l=1}^{4} M_{LC}^{(i,l)} \tag{21}$$

We compute the arc-straight mutual inductance similarly to Eq. (18). Because the two coils may have different dimensions, we exchange the orders of the two segments:

$$M_{CL}^{(k,j)} = \frac{\mu_0}{4\pi}\int_0^{\frac{\pi}{2}}\int_0^1 \frac{\mathbf{t}_1^{(k)}(\theta)\cdot\left(\mathbf{R}\mathbf{v}_2^{(j)}\right)d\theta ds}{D_{CL}^{(k,j)}(\theta,s)} \tag{22}$$

Thus, the arc-straight mutual inductance can be expressed as:

$$M_{CL} = \sum_{k=1}^{4}\sum_{j=1}^{4} M_{CL}^{(k,j)} \tag{23}$$

For the k-th arc segment of the primary coil and the l-th arc segment of the secondary coil, the mutual inductance is:

$$M_{CC}^{(k,l)} = \frac{\mu_0}{4\pi} r_1 r_2 \int_0^{\frac{\pi}{2}}\int_0^{\frac{\pi}{2}} \frac{\mathbf{t}_1^{(k)}(\theta)\cdot\left(\mathbf{R}\mathbf{t}_2^{(l)}(\phi)\right)}{D_{CC}^{(k,l)}(\theta,\phi)} d\theta d\phi \tag{24}$$

The distance function is:

$$D_{CC}^{(k,l)}(\theta,\phi) = \left\|\mathbf{r}_1^{(k)}(\theta) - \mathbf{R}\mathbf{r}_2^{(l)}(\phi) - \mathbf{T}\right\| \tag{25}$$

The total arc-arc mutual inductance is:

$$M_{CC} = \sum_{k=1}^{4}\sum_{l=1}^{4} M_{CC}^{(k,l)} \tag{26}$$

Then, for rounded rectangular coils with N_1 and N_2 turns positioned arbitrarily in space, the total mutual inductance is:

$$M_{\text{total}} = \sum_{p=1}^{N_1}\sum_{q=1}^{N_2} M_{pq} = \sum_{p=1}^{N_1}\sum_{q=1}^{N_2}\left\{\sum_{i=1}^{4}\sum_{j=1}^{4}\left[M_{LL}^{(i,j)}(p,q) + M_{LC}^{(i,l)}(p,q) + M_{CL}^{(k,j)}(p,q) + M_{CC}^{(k,l)}(p,q)\right]\right\} \tag{27}$$

where $M_{LL}^{(i,j)}(p,q)$, $M_{LC}^{(i,l)}(p,q)$, $M_{CL}^{(k,j)}(p,q)$, $M_{CC}^{(k,l)}(p,q)$ are obtained from Eqs. (15), (18), (22), and (24). N_1 and N_2 are the numbers of turns of the two coils, and p and q denote the p-th turn of the primary coil and the q-th turn of the secondary coil.

We implement the calculation in MATLAB 2024a. Fig. 6 shows the calculation flowchart.

As illustrated in Fig. 6, the procedure first specifies the coil parameters and transformation data. Then, it transforms the secondary coil segments using Eq. (5) and uses a double loop over all turn pairs to compute M_{ij} via numerical integration of the four interaction components. After the loop terminates, it accumulates and outputs the total mutual inductance M_{total} (Eq. (27)). We evaluate all double integrals in Eqs. (15), (18), (22), and (23) numerically using the integral2 function in MATLAB, which implements an adaptive Gauss-Kronrod quadrature with relative tolerance 1×10^{-6} and an absolute tolerance 1×10^{-9}. We apply the same numerical scheme to all four interaction types. For a single spatial configuration, the MATLAB computation time for the full multi-turn coil is approximately 2 seconds. By contrast, an equivalent finite element method (FEM) simulation in Ansys Maxwell requires about 20–30 minutes per configuration.

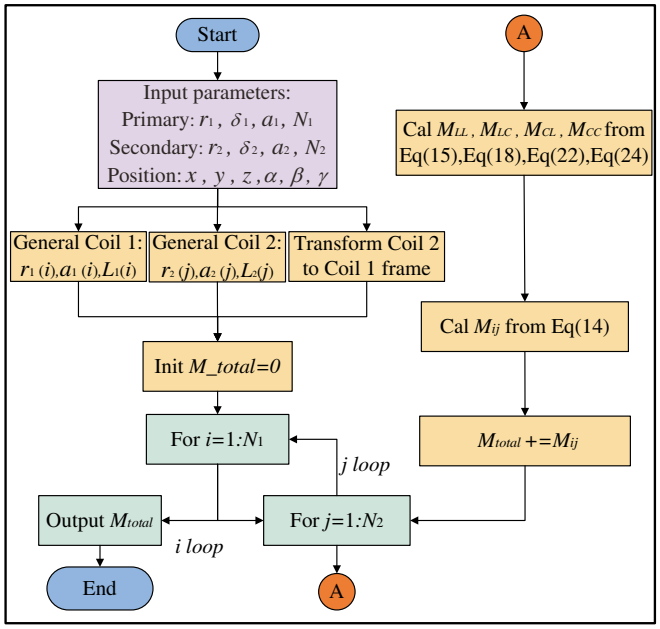

FIGURE 6. Computational flowchart.

A tolerance sensitivity test shows that relaxing the relative tolerance from 10^{-6} to 10^{-5} changes the total mutual inductance by less than 0.5%, confirming that the chosen tolerance provides excellent convergence without unnecessary overhead. Moreover, a single arc-arc (M_{CC}) evaluation takes about 4 times longer than a straight-straight (M_{LL}) evaluation due to the higher complexity of its integrand, but the overall per-configuration time remains about 2 seconds.

3. SIMULATION AND EXPERIMENTAL VERIFICATION

3.1. Simulation and Analysis of Mutual Inductance of Rounded Rectangular Coils

To validate the proposed formula, we selected two coils with different parameters. We conducted mutual inductance tests under various conditions, including displacement, rotation, and arbitrary spatial positions. The parameters of the coils are listed in Table 1. Note that although the analytical model uses the thin-wire approximation and does not directly include wire diameter as a variable, this parameter remains essential. It defines the centerline geometry of each turn and is needed to fabricate the physical coils used in experiments and FEM simulations.

TABLE 1. Coil parameter settings.

Coil	Starting position x (mm)	Rounded radius r (mm)	Wire diameter w (mm)	Pitch δ (mm)	Number of turns N
A	40	6	1.5	2.5	8
B	30	5	2	4	7
C	50	5	2	2.8	18
D	40	9	1.5	2.5	8
E	40	12	1.5	2.5	8

TABLE 2. Comparison between coils with rounded corners and those without rounded corners.

Coil	Parameters	M_1/μH	M_2/μH	
	X, Y, Z (mm) α, β, γ (°)	FEM	FEM	CAL
A, A	40, 0, 0; 0, 0, 0	2.519	2.498	2.501
A, A	40, 20, 20; 0, 0, 0	2.041	2.029	2.033
A, A	40, 0, 0; 15, 15, 0	2.590	2.566	2.574
D, D	40, 0, 0; 0, 0, 0	2.518	2.486	2.490
D, D	40, 20, 20; 0, 0, 0	2.041	2.019	2.023
D, D	40, 0, 0; 15, 15, 0	2.588	2.543	2.565
E, E	40, 0, 0; 0, 0, 0	2.518	2.465	2.473
E, E	40, 20, 20; 0, 0, 0	2.040	1.998	2.007
E, E	40, 0, 0; 15, 15, 0	2.588	2.538	2.549

To verify the proposed analytical method, we used coils A and B as the primary and secondary coils, respectively, for displacement and rotation validation. The calculated mutual inductance refers to the value obtained using the proposed formula. We obtained simulation results using Ansys Maxwell 3D on a computer with 32 GB RAM. We set the solver type to "Magnetostatic", assumed a uniform current distribution on the coil cross-section, used the mesh assignment method "Based on Length", and set the circular boundary to more than five times the coil length.

To evaluate how the rounded corner radius affects mutual inductance accuracy, we used three coil sizes (A, D, E) with different radii. We calculated mutual inductance using the proposed method and compared it with FEM results under identical spatial configurations. In Table 2, M_1 and M_2 represent the FEM results without and with rounded corners, while "CAL" denotes the analytical result from the proposed method. Table 3 presents the relative errors: Error1 $= |M_1 - \text{CAL}|/\text{CAL} \times 100\%$ and Error2 $= |M_2 - \text{CAL}|/\text{CAL} \times 100\%$. The six parameters X, Y, Z are the translational displacements of the secondary coil along the reference X, Y, Z axes (see Fig. 4), and α, β, γ are the rotation angles about the X, Y, Z axes following the Z-Y-X Euler order defined in Section 2.1.

As shown in Table 2 and Table 3, for different spatial orientations, the analytical model that considers rounded corners achieves errors within 0.5%, whereas neglecting rounded corners increases the error up to 1.82%. This confirms the necessity and superiority of accurately modeling the rounded corner geometry.

TABLE 3. Relative errors of mutual inductance calculations with and without considering rounded corners.

Coil	Parameters X, Y, Z (mm) α, β, γ (°)	Error1	Error2
A, A	40, 0, 0; 0, 0, 0	0.72%	0.12%
A, A	40, 20, 20;0, 0, 0	0.39%	0.15%
A, A	40, 0, 0; 15, 15, 0	0.62%	0.32%
D, D	40, 0, 0; 0, 0, 0	1.12%	0.16%
D, D	40, 20, 20; 0, 0, 0	0.89%	0.20%
D, D	40, 0, 0; 15, 15, 0	0.90%	0.47%
E, E	40, 0, 0; 0, 0, 0	1.82%	0.32%
E, E	40, 20, 20; 0, 0, 0	1.64%	0.40%
E, E	40, 0, 0; 15, 15, 0	1.53%	0.43%

TABLE 4. Test cases near and below the thin-wire validity boundary.

Coil	Z (mm)	$M_{\text{FEM}}/\mu H$	$M_{\text{CAL}}/\mu H$	Error (%)
A, B	6.0	5.952	5.885	1.14%
A, B	4.5	6.355	6.289	1.68%
A, B	3	6.866	6.735	1.94%
A, B	2	7.289	7.057	3.29%

To assess the method under near-singular conditions, we tested coil A with several axial spacings given $d/w < 5$ ($X = Y = 0$ mm, $\alpha = \beta = \gamma = 0°$). Table 4 lists the calculated mutual inductance and FEM results.

Table 4 shows how the error evolves as the axial spacing decreases. The relative error grows progressively when d/w drops from 5 to 2, reaching about 3.3% at the smallest tested spacing. This trend confirms that the method remains stable down to very close separation, though the error becomes more pronounced when coils are almost touching. For practical WPT applications, where coils are typically well separated, the thin-wire model gives high accuracy; for cases requiring extreme proximity, a GMD correction is recommended.

To further validate the proposed analytical model under more complex spatial orientations, we performed mutual inductance calculations under different rotation and misalignment conditions and compared them with finite element simulation results, as shown in Fig. 7.

Figure 7(a) shows two lateral displacement tests: one with an axial spacing of $Z = 60$ mm, $Y = 0$ mm, and the other with

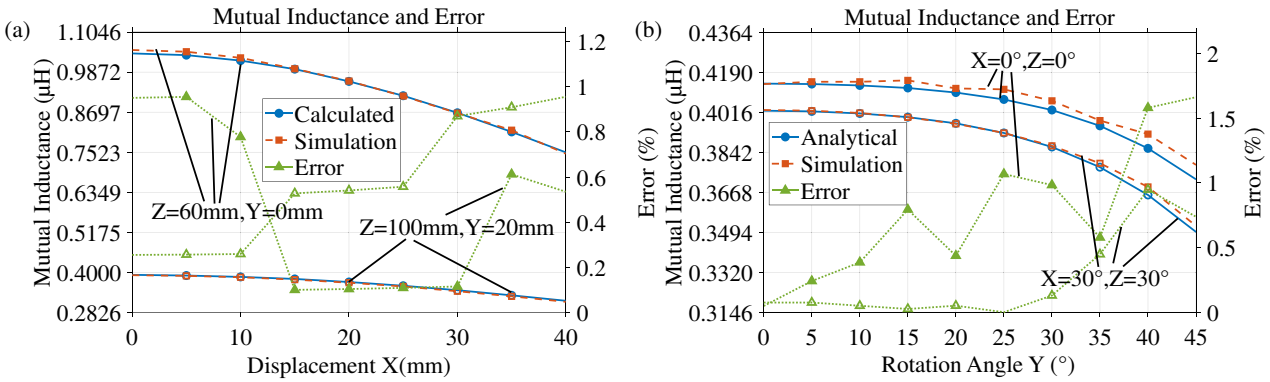

FIGURE 7. Comparison of calculated (blue solid line with circles) and simulated (red dashed line with squares) mutual inductance results and errors (green dotted line with triangles) under different conditions: (a) displacement along the X-axis, (b) rotation about the Y-axis.

$Z = 100$ mm, $Y = 20$ mm. In both cases, the X-axis displacement varies from 0 to 40 mm while the axial spacing remains fixed. The second category is relative rotation. Fig. 7(b) shows two cases. First, with fixed axial displacement $Z = 100$ mm and the two coils parallel and aligned ($\alpha = 0°$, $\beta = 0°$), we rotate about the Y-axis from 0° to 45°. Second, with the same axial displacement but both coils rotated by 30° about the X-axis and Z-axis ($\alpha = 30°$, $\beta = 30°$), we again apply rotation about the Y-axis from 0° to 45°.

Under various typical operating conditions, including lateral displacement, axial displacement, and both single-axis and compound rotation, the maximum relative error does not exceed 1.5%, and the average relative error is less than 0.8%. These results fully demonstrate the good calculation accuracy and robustness of the analytical model based on geometric decomposition, which can accurately and reliably predict the mutual inductance characteristics of rounded rectangular coils under arbitrary spatial orientations.

3.2. Rounded Rectangular Coil Mutual Inductance Experimental Test

To verify the feasibility of the proposed method, we fabricated two rounded rectangular coils using Litz wire. We constructed the experimental platform as shown in Fig. 8. The platform consisted of an LCR bridge (TL2818D), acrylic plates, and the two fabricated coils.

In this experiment, we used the method introduced by Acero et al. to measure mutual inductance [22]. The series connection method is a classic approach for measuring mutual inductance between two coils. By changing the connection mode of the two coils, the total inductance under different connection configurations can be measured. The LCR bridge (TL2818D) has a specified basic accuracy of ±0.5% for inductance measurements. We report each mutual inductance value as the average of three repeated measurements; the maximum standard deviation across all test points is 0.8%. Positioning uncertainties are ±0.2 mm for linear displacements (using mechanical stages) and ±1° for rotations (using protractor scales). We maintained the ambient temperature at 20 ± 1°C to avoid thermal drift.

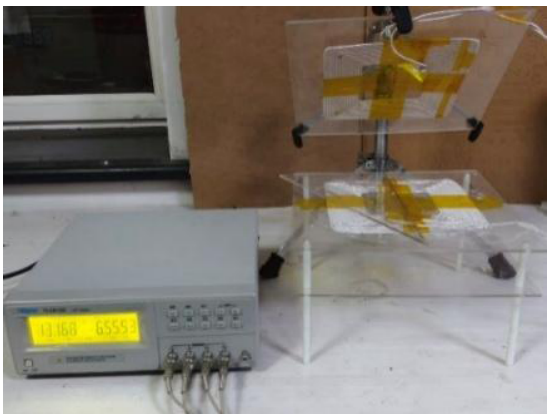

FIGURE 8. Experimental platform for mutual inductance measurement.

When the two coils are connected in series aiding, the inductance is $L_{\text{series}} = L_1 + L_2 + 2M$; when they are connected in series opposing, the inductance is $L_{\text{oppose}} = L_1 + L_2 - 2M$. By measuring the inductances in series aiding and series opposing, the mutual inductance is obtained as $M = (L_{\text{series}} - L_{\text{oppose}})/4$.

Figure 9 shows the mutual inductance curves from finite element simulation, analytical calculation, and experimental measurement under different conditions. Fig. 9(a) shows the mutual inductance as the coil undergoes lateral displacement from 0 to 50 mm, with measurements recorded every 5 mm. The lateral displacement was varied for $Y = 0$ mm, $Y = 20$ mm, $Y = 40$ mm. Fig. 9(b) shows the mutual inductance as the coil was displaced along the Z-axis from $Z = 20$ mm to $Z = 120$ mm with measurements taken every 10 mm. The mutual inductance was measured for lateral displacements of 15 mm and 30 mm. Fig. 9(c) shows the mutual inductance as the coil rotates about the Z-axis from 0° to 90°, with measurements taken every 15°, while maintaining a constant $Z = 60$ mm. Measurements were taken with lateral displacements of ($X = 25$ mm, $Y = 0$ mm) and ($X = 25$ mm, $Y = 25$ mm). Fig. 9(d) shows the mutual inductance as we rotate the coil about the X-axis from 0° to 90° while keeping the lateral displacement fixed, taking measurements at axial distances $Z = 120$ mm, $Z = 140$ mm, $Z = 160$ mm.

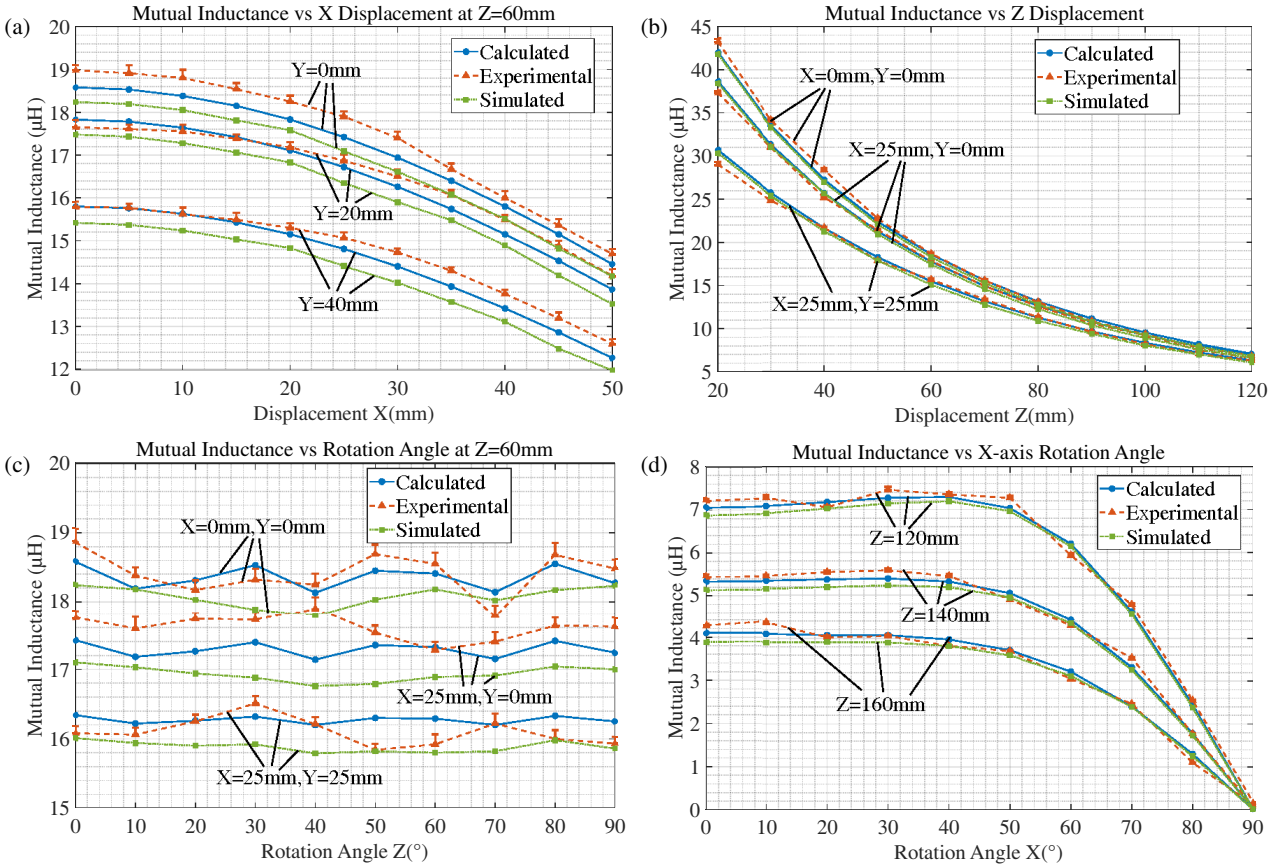

FIGURE 9. Calculated (blue solid line with circles), simulated (green dotted line with squares), and experimental (red dashed line with triangles) characteristic curves of mutual inductance of rounded rectangular coil under multiple degrees of freedom displacement, (a) displacement along the X-axis, (b) displacement along the Z-axis, (c) rotation about the Z-axis, (d) rotation about the X-axis.

As shown in Fig. 9(a), the mutual inductance gradually decreases with increasing lateral displacement. The analytical calculations agree well with the finite element simulation results, showing an average relative error of approximately 0.8% compared with experimental measurements and a maximum error not exceeding 1.5%. This indicates that the proposed method is reliable under lateral displacement conditions. For Fig. 9(b), the mutual inductance decays exponentially as the spacing increases. The analytical calculations agree closely with the experimental measurements, with an average relative error below 1.5%. This confirms that the proposed method maintains high accuracy over a wide range of spacings. For Fig. 9(c), the experimental results show that when the secondary coil rotates about the Z-axis, the mutual inductance varies only slightly. Because the tested coil is square, rotation about the vertical axis does not alter the effective area projected onto the coil plane. For a non-square coil, a rotation would cause the mutual inductance to vary periodically with angle. For Fig. 9(d), the mutual inductance decreases monotonically with increasing tilt angle, and the analytical results remain within 2.0% of the experimental values.

Based on the multiple sets of experimental results presented above, the maximum relative error between the analytical method and experimental measurements is consistently within 2.5%, and it remains within 1.5% compared with the finite element simulation results, demonstrating that the method possesses high practical engineering accuracy. It should be noted that the experimental validation in this section was performed using coil C. For coils with larger corner radii (e.g., coil E), experimental validation remains future work due to fabrication constraints; however, the FEM validation provided in Section 3.1 (Tables 2, 3, and Table 4) confirms the method's accuracy for such geometries.

Regarding the proposed analytical calculation method for mutual inductance of planar, rounded rectangular spiral coils, the possible reasons for the error are as follows:

(1) The analytical calculation is based on the thin-wire assumption. When the distance between coil segments decreases, the influence of the wire cross-section becomes non-negligible.

(2) Floating-point calculation errors become amplified through Euler angle transformations, especially under large rotations.

(3) When two segments approach parallelism, the distance varies dramatically over the integration interval, leading to a near-singular integrand.

(1) Introduce a correction factor based on the geometric mean distance (GMD) method to account for the finite cross-section.

(2) Replace Euler angles with a quaternion representation to reduce numerical errors.

TABLE 5. Comparison with existing works on mutual inductance modeling of planar coils.

Reference	Rounded corners considered	Arbitrary 3D orientation	Key novelty
[9]	Yes	No	Rounded rectangular coils
[12]	No	Yes	General 6-DoF for spiral coils
[13]	No	Yes	Regular polygonal coils
[21]	No	No	Historical basis: segment superposition
[23]	Yes	No	Rounded rectangular coils with rectangular cross-section
This work	Yes	Yes	First combination of rounded corners + arbitrary 3D orientation

(3) Implement an adaptive integration scheme with singularity subtraction for near-singular integrands.

4. CONCLUSION

As summarized in Table 5, the primary novelty of this work lies in providing a fully analytical framework that simultaneously accounts for the rounded corner geometry and arbitrary 3D orientations, a combination not found in previous studies.

The method maintains average errors below 1.5% compared with FEM (validated for corner radii up to 12 mm) and below 2.5% compared with experiments (validated for a corner radius of 5 mm), confirming its ability to eliminate systematic errors from ideal rectangle approximations, and requires about 2 seconds per configuration in MATLAB versus 20–30 minutes in FEM.

Regarding multi-turn interaction effects, this study approximates the multi-turn coil as a set of concentric single-turn loops. This thin-wire approximation is common in analytical mutual inductance calculations and works well for low to medium-frequency wireless power transfer systems (e.g., 85 kHz for electric vehicle charging) that use Litz wire. However, at higher frequencies, these effects may become non-negligible. Therefore, future work will incorporate frequency-dependent resistance models and mutual coupling corrections between adjacent turns to further enhance the accuracy of the proposed method for practical coil designs.

REFERENCES

[1] Wu, J., B. Wang, W. S. Yerazunis, and K. H. Teo, "Wireless power transfer with artificial magnetic conductors," in *2013 IEEE Wireless Power Transfer (WPT)*, 155–158, Perugia, Italy, 2013.

[2] Xia, C., J. Yan, G. Ren, *et al.*, "Simultaneous wireless power and reverse signal transmission technology based on harmonic communication," *Proceedings of the CSEE*, Vol. 44, No. 13, 5297–5308, 2024.

[3] Chen, W., Y. Liu, X. Yan, *et al.*, "Reactive shielding of four matching capacitors for resonant wireless power transfer in cardiac pacemakers," *Transactions of China Electrotechnical Society*, Vol. 40, No. 14, 4382–4394, Jul. 2025.

[4] Manos, K., Y. Rao, T. Zhao, K. Liu, D. Zhou, C. Nguyen, E. Chen, G. H. Paulino, and M. Chen, "Wireless actuation of magnetic robots with a modular 60 mT 3-D helmholtz coil system," in *2025 IEEE Applied Power Electronics Conference and Exposition (APEC)*, 1274–1278, Atlanta, GA, USA, 2025.

[5] Hsieh, Y.-C., Z.-R. Lin, M.-C. Chen, H.-C. Hsieh, Y.-C. Liu, and H.-J. Chiu, "High-efficiency wireless power transfer system for electric vehicle applications," *IEEE Transactions on Circuits and Systems II: Express Briefs*, Vol. 64, No. 8, 942–946, Aug. 2017.

[6] Baua, S., R. K. Amineh, and N. S. Artan, "Wireless power transfer with multi-layer planar spiral coils as secondary coils," in *2018 IEEE Wireless Power Transfer Conference (WPTC)*, 1–4, Montreal, QC, Canada, 2018.

[7] Nottiani, D. G. and F. Leccese, "A simple method for calculating lumped parameters of planar spiral coil for wireless energy transfer," in *2012 11th International Conference on Environment and Electrical Engineering*, 869–872, Venice, Italy, 2012.

[8] Luo, Z. and X. Wei, "Analysis of square and circular planar spiral coils in wireless power transfer system for electric vehicles," *IEEE Transactions on Industrial Electronics*, Vol. 65, No. 1, 331–341, Jan. 2018.

[9] Jiang, Y., Y. Wu, Y. Li, Z. Xiao, N. Wang, M. Wu, X. Wang, and Y. Tang, "Precise modeling for the inductance of rounded rectangular coils in wireless power transfer systems," in *IECON 2023 — 49th Annual Conference of the IEEE Industrial Electronics Society*, 1–7, Singapore, 2023.

[10] Liu, X., Y. Cao, C. Xia, *et al.*, "Optimization of hybrid compensation topology and anti-offset performance of wireless power transfer system based on QRQP coil," *Transactions of China Electrotechnical Society*, Vol. 40, No. 12, 3828–3841, Jun. 2025.

[11] Wang, W., L. Wang, P. Zhang, *et al.*, "Research on performance optimization of WPT system based on improved DSQP coil," *Electronic Design Engineering*, Vol. 33, No. 24, 36–41, Dec. 2025.

[12] Liu, S., J. Su, J. Lai, J. Zhang, and H. Xu, "Precise modeling of mutual inductance for planar spiral coils in wireless power transfer and its application," *IEEE Transactions on Power Electronics*, Vol. 36, No. 9, 9876–9885, Sep. 2021.

[13] Altun, H. and N. Pirinççi, "A novel analytical model for mutual inductance calculations between two nonidentical N-sided polygonal planar coils arbitrarily positioned in 3-D space for wireless power transfer," *IEEE Transactions on Power Electronics*, Vol. 38, No. 8, 10 396–10 411, Aug. 2023.

[14] Li, Z., M. Bao, L. Kong, *et al.*, "Calculation of mutual inductance between rectangular coils at arbitrary positions of porous magnetic media for wireless energy transmission systems," *Transactions of China Electrotechnical Society*, Vol. 40, No. 24, 7863–7878, 2025.

[15] Zheng, M., Z. Luo, and Z. Li, "Design of inductive magnetic sensor for space magnetic field measurement," in *2024 4th International Conference on Electronics, Circuits and Information Engineering (ECIE)*, 91–97, Hangzhou, China, 2024.

[16] Wu, D. and H. Feng, "A novel method for calculating the mutual inductance between two perpendicular coils in wireless power transfer," *International Journal of Circuit Theory and Applications*, Vol. 51, No. 10, 4550–4564, 2023.

[17] Yu, X., J. Feng, L. ZHu, and Q. Li, "Modelling of a planar omnidirectional wireless power transfer system," in *2024 IEEE Applied Power Electronics Conference and Exposition (APEC)*, 2609–2615, Long Beach, CA, USA, 2024.

[18] Pandey, A., S. Samanta, and A. Edpuganti, "Accurate modeling approach of litz-wire based planar DD spiral coils for WPT applications," in *2024 IEEE International Conference on Power Electronics, Drives and Energy Systems (PEDES)*, 1–6, Mangalore, India, 2024.

[19] Qian, L., M. Chen, K. Cui, G. Shi, J. Wang, and Y. Xia, "Modeling of mutual inductance between two misalignment planar coils in wireless power transfer," *IEEE Microwave and Wireless Components Letters*, Vol. 30, No. 8, 814–817, Aug. 2020.

[20] Zhang, K., "Calculation and analysis of plane magnetic field distribution and inductance of circular coil," *Jiangsu Science & Technology Information*, Vol. 39, No. 24, 45–49, Aug. 2022.

[21] Greenhouse, H., "Design of planar rectangular microelectronic inductors," *IEEE Transactions on Parts, Hybrids, and Packaging*, Vol. 10, No. 2, 101–109, Jun. 1974.

[22] Acero, J., C. Carretero, I. Lope, R. Alonso, O. Lucia, and J. M. Burdio, "Analysis of the mutual inductance of planar-lumped inductive power transfer systems," *IEEE Transactions on Industrial Electronics*, Vol. 60, No. 1, 410–420, Jan. 2013.

[23] Wu, D., Q. Sun, X. Wang, and F. Cheng, "Calculation of self-and mutual inductances of rounded rectangular coils with rectangular cross-sections and misalignments," *IET Electric Power Applications*, Vol. 12, No. 7, 1014–1019, 2018.